HOSTED BY

ELSEVIER

Available online at www.sciencedirect.com

ScienceDirect

Journal of Magnesium and Alloys 3 (2015) 210–217
www.elsevier.com/journals/journal-of-magnesium-and-alloys/2213-9567

Full Length Article

Age hardening, fracture behavior and mechanical properties of QE22 Mg alloy

F. Khan MD, S.K. Panigrahi *

Department of Mechanical Engineering, Indian Institute of Technology Madras, Chennai 600036, India

Received 7 March 2015; revised 16 August 2015; accepted 25 August 2015

Available online 28 September 2015

Abstract

The microstructure, mechanical properties and fracture behavior of an as-received QE22 alloy have been investigated under different thermal conditions, including solution treated (ST), under aged (UA), peak aged (PA) and over aged (OA) conditions. A significant increase in hardness of 27%, yield strength of 60% and ultimate tensile strength of 19% was observed in peak aged sample as compared to solution treated sample. The improvements of mechanical strength properties are mainly associated with the metastable λ and β′ precipitates. Grain growth was not observed in the ST samples after subjecting to UA and PA treatments due to the presence of eutectic $Mg_{12}Nd$ particles along the grain boundaries. In over aged sample, significant grain growth occurred because of dissolution of eutectic phase particles. Different natures of crack initiation and propagation were observed under different thermal conditions during tensile testing at room temperature. The mode of failure of solution treated sample is transgranular, cleavage and twin boundary fractures. A mixed mode of transgranular, intergranular, cleavage and twin boundary failure is observed in both peak aged and over aged samples.

Keywords: Magnesium alloy (QE22); Age hardening behavior; Microstructure; Mechanical properties; Fracture

1. Introduction

Magnesium alloys have received an increasing interest in the last decade for potential applications in the automotive, aerospace, defense and electronic industries. An increased usage of these alloys depends on enhancing their mechanical properties further. One of the potential conventional methods of improving the strength properties of magnesium alloys is development of age hardenable alloys.

Among various age hardenable magnesium alloys, Mg-Ag-Re alloys are most famous because of their very good thermal stability, remarkable age hardening response, good creep resistance, good tensile strength and fatigue strength [1]. These alloys are mainly used in automotive, military and aircraft industries such as gear box casings, engine casings, wheels and rotor heads in helicopters [2]. The fracture behavior of these alloys is also important in understanding the relationship between microstructure and mechanical properties, as it determines the fracture strength and elongation. Few researchers have attempted to correlate the relation between fracture behavior and mechanical properties of Mg-Y-Nd alloy, Mg-Gd-Y-Zr alloy and Mg-Gd-Er alloy [3–7]. However similar attempt on Mg-Ag-Nd alloy has not been studied so far. Even though, few researchers have studied the phase transformations and age hardening behavior of different Mg-Ag-Re based alloys and composites [8–13], there is still a degree of uncertainty in the literature about the precipitation sequence, structure and composition of hardening phases of these alloys.

This paper mainly studies the evolution of microstructure, fracture behavior and mechanical property in magnesium silver rare earth (Mg-Ag-Nd-Zr) commercial alloy (commonly named QE22) when subjected to different thermal treatments. The objective of this work is to establish relationship between precipitation, microstructure, mechanical properties and fracture behavior.

2. Experimental procedure

The as-received QE22 alloy of 25 mm thick plate was procured from Magnesium Elektron, Manchester, UK. The chemical composition of this alloy is provided in Table 1. The

* Corresponding author. Department of Mechanical Engineering, Indian Institute of Technology Madras, Chennai 600036, India. Tel.: +91 44 22574742; fax: +91 44 22574652.

E-mail address: skpanigrahi@iitm.ac.in (S.K. Panigrahi).

http://dx.doi.org/10.1016/j.jma.2015.08.002
2213-9567/

Table 1
Chemical composition of the as-received material QE22 alloy.

Element (wt%)	Mg	Ag	Nd	Zr
As received	93.25	4.08	2.07	0.6

chemical composition of the as-received material is tested through optical emission spectroscopy (OES). The samples with required dimension were solution treated at 525 °C for 8 hours, quenched into cold water, and then isothermally aged at 200 °C for various periods of time. In order to prevent oxidation, the samples were kept in quartz crystal glass tube prior to solution treatment. The heat treated samples were subjected to mechanical polishing by using different emery grit sizes, followed by diamond polishing and etched with picric acid solution. For the microstructure observation, an inverted metallographic microscope Quama 5000 series and a Quanta 200 scanning electron microscope with EDAX attachment were used. The polished samples with and without heat treatment were taken to microhardness testing to determine the hardness value. The test was carried out on Vickers Microhardness testing machine with a load of 200 g for 10 s. Phase analysis was carried out with X-ray diffraction (XRD). Thin foils of QE22 alloy (less than 100 μm) samples are prepared to study the morphology of the precipitates from transmission electron microscopy. Thin foils were twin jet polished with electrolyte (99% pure ethanol + 1% Perchloric acid) followed by ion milling. Phillips 200 kV model transmission electron microscopy was employed to conduct these experiments. At most care was taken to prevent oxidation of magnesium samples after electrolyte polishing.

The tensile tests were performed at a cross head speed of 1 mm/min at room temperature. The samples for tensile tests had a gauge length of 5 mm, width of 2 mm and thickness of 2 mm. Three specimens were used for each test condition to ensure the reproducibility of data. The fractured specimens were sectioned longitudinally and examined mode of failure using optical microscopy (OM). The fracture surfaces of the failed tensile specimens were examined using scanning electron microscopy.

3. Results and discussions

3.1. Microstructure

The SEM-BSE microstructure of the solution treated sample is shown in Fig. 1. The chemical composition of the ST sample and eutectic phase is shown in Table 2.

The microstructure of the ST sample is mainly composed of equiaxed grains surrounded by eutectic network and second phase. The average grain size (GS) and hardness of the solution treated sample are observed as 52 μm and 64 Hv respectively. Linear intercept method was used to obtain average grain size. The observed eutectic phase is rich in Ag and Nd (Table 2) which indicates the occurrence of an Mg-Ag-Re ternary phase.

3.2. Age hardening behavior

The as-received QE22 Mg alloy is an age hardenable alloy. To know the peak aging temperature of this alloy, solution

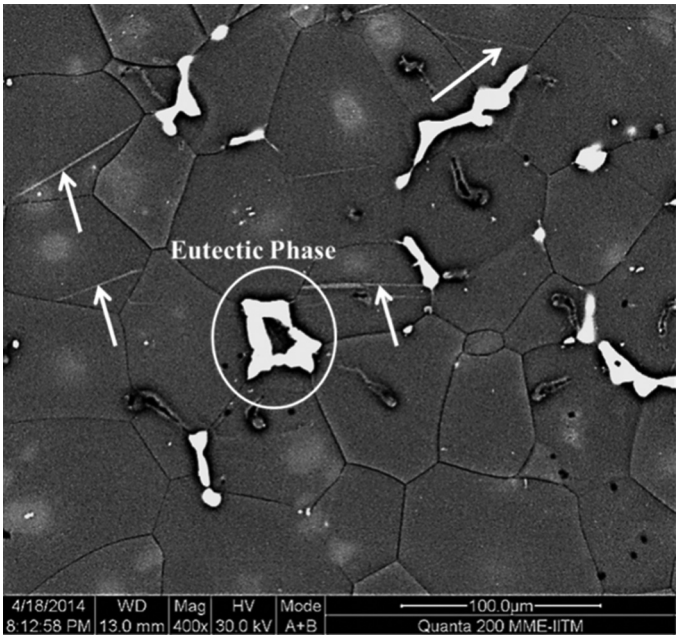

Fig. 1. Microstructure of solution treated QE22 alloy (arrow indicates twins).

treated (ST) samples are aged for 1 hour at different aging temperatures from 50 °C to 500 °C, followed by microhardness testing. Fig. 2 shows the age hardening response of the ST QE22 alloy. An increase in microhardness trend is observed in the ST QE22 alloy with increase in aging temperature up to

Table 2
Chemical composition of the ST QE22 alloy and eutectic phase.

Element (wt%)	Mg	Ag	Nd	Zr
Solution treated	92.19	3.23	2.19	2.39
Eutectic Phase	66.40	10.58	20.35	2.66

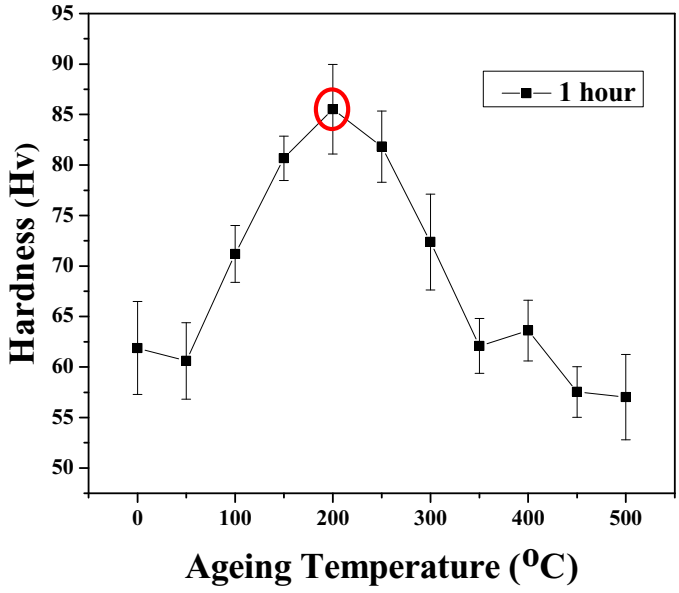

Fig. 2. Effect of aging temperature on hardness of the ST QE22 alloy for 1 hour of aging duration.

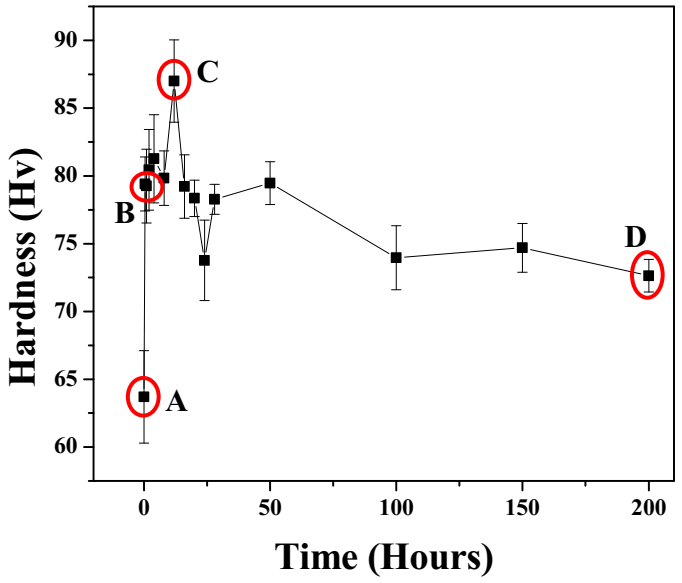

Fig. 3. Age hardening behavior of the ST QE22 alloy at 200 °C: (A) solution treated (ST); (B) under aging (UA); (C) peak aging (PA); (D) over aging (OA) condition.

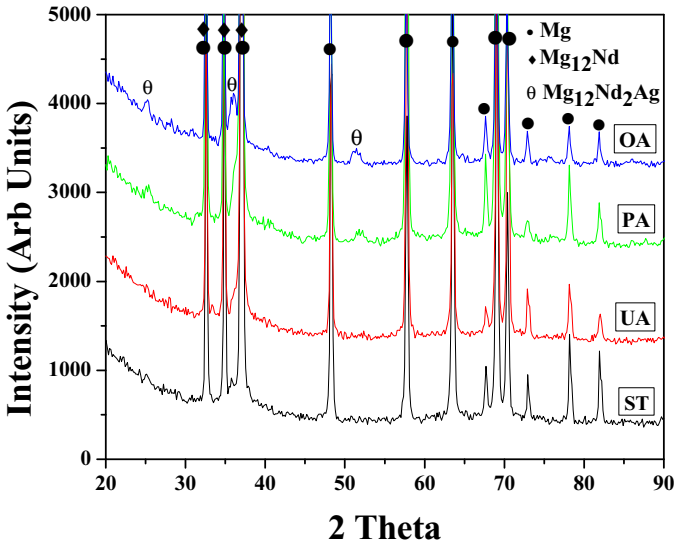

Fig. 4. XRD pattern of the QE22 alloy at different aging conditions: solution treated (ST); under aged (UA); peak aged (PA); over aged (OA).

200 °C and then decreases. Therefore, 200 °C is selected for further age hardening studies. The age hardening behavior of the ST QE22 alloy at temperature of 200 °C is shown in Fig. 3. The samples are aged isothermally at 200 °C for various time intervals from 0.5 to 200 hours, followed by air cooling. Prior to aging, the initial hardness of the solution treated alloy is 64 Hv. During aging, a significant increase in hardness is observed up to 12 hours and then it decreases. At peak aging condition, the hardness value is observed as 87 Hv.

Faster increase in hardness and smaller time to peak (about 12 h) is observed in the present alloy which seems to be a potential material for industrial application. After obtaining the peak hardness at 12 hours, the prolonged aging leads to only a slight reduction in hardness. Moreover, the alloy aged at 200 °C shows a broad width of stable hardness for a long duration from 12 to 200 h with an average micro hardness not less than 74 Hv. From the age hardening plot, four aging conditions at aging times of 0 h, 0.5 h, 12 h and 200 h are selected which corresponds solution treated (ST), under aged (UA), peak aged (PA) and over aged (OA) treatments respectively. The ST samples are subjected to the above mentioned treatments to obtain UA, PA and OA samples. The post microstructural analysis and mechanical properties were evaluated in the age hardened samples to understand the mechanism of age hardening behavior of the present alloy.

Fig. 4 shows the XRD results of ST, UA, PA and OA samples. In all the samples α-Mg and $Mg_{12}Nd$ peaks are detected. A ternary precipitate phase of $Mg_{12}Nd_2Ag$ is observed in PA and OA samples. This ternary phase is not observed in XRD plots of ST and UA samples. During high temperature solution treatment and quenching, Nd and Ag solutes might have dissolved in Mg matrix and retained in metastable state. Upon heat treating the ST samples to PA and OA treatment, precipitation of $Mg_{12}Nd_2Ag$ phase occurred which is responsible for increase in hardness in both of the thermal treated samples than that of ST sample.

Fig. 5 shows the microstructures of the ST, UA, PA and OA samples. The microstructure of the ST, UA and PA sample contains equiaxed grains with eutectic phase which is decorated along the grain boundaries. The SEM-EDAX result (Table 2) indicates that the observed eutectic phase is Mg-Ag-RE ternary phase. This result contradicts with XRD result of ST sample. The XRD result reveals that the ST material contains binary $Mg_{12}Nd$ eutectic phase. The possible reason may be due to similar size of atomic radius between magnesium (r_{Mg}: 0.162 nm) and silver atoms (r_{Ag}: 0.144 nm). Due to this reason, the atoms of silver can replace the atoms of magnesium without disturbing the crystal structure of intermetallic eutectic phase [10,11]. Therefore, the possible eutectic phase which is decorated along the grain boundaries of the all the four thermal treated samples may be of binary $Mg_{12}Nd$ phase. The average grain sizes of all the three thermal treated (ST, UA and PA) samples are almost similar and lie in the range of 50 ± 3 μm. The higher thermal stability of UA and PA samples is due to the presence of eutectic phase along the grain boundaries which provides pinning action on the grain boundaries leading to suppression of grain growth. Significant grain growth is observed in OA sample (74 μm). The eutectic phase which was observed along the grain boundaries of ST, UA, PA samples is not observed in OA sample. Therefore, the occurrence of grain growth in OA sample is due to dissolution of the eutectic phase which is responsible for retardation of grain growth in UA and PA states. The presence of twins is also observed in all the thermal treated samples. The order of twin fraction in all the four thermal treated samples is as follows: ST > UA > PA > OA. In ST sample, the cast as-received material is solution treated at 525 °C for 8 hours followed by cold water quenching. Due to rapid quenching from high temperature, internal stresses developed in the material which

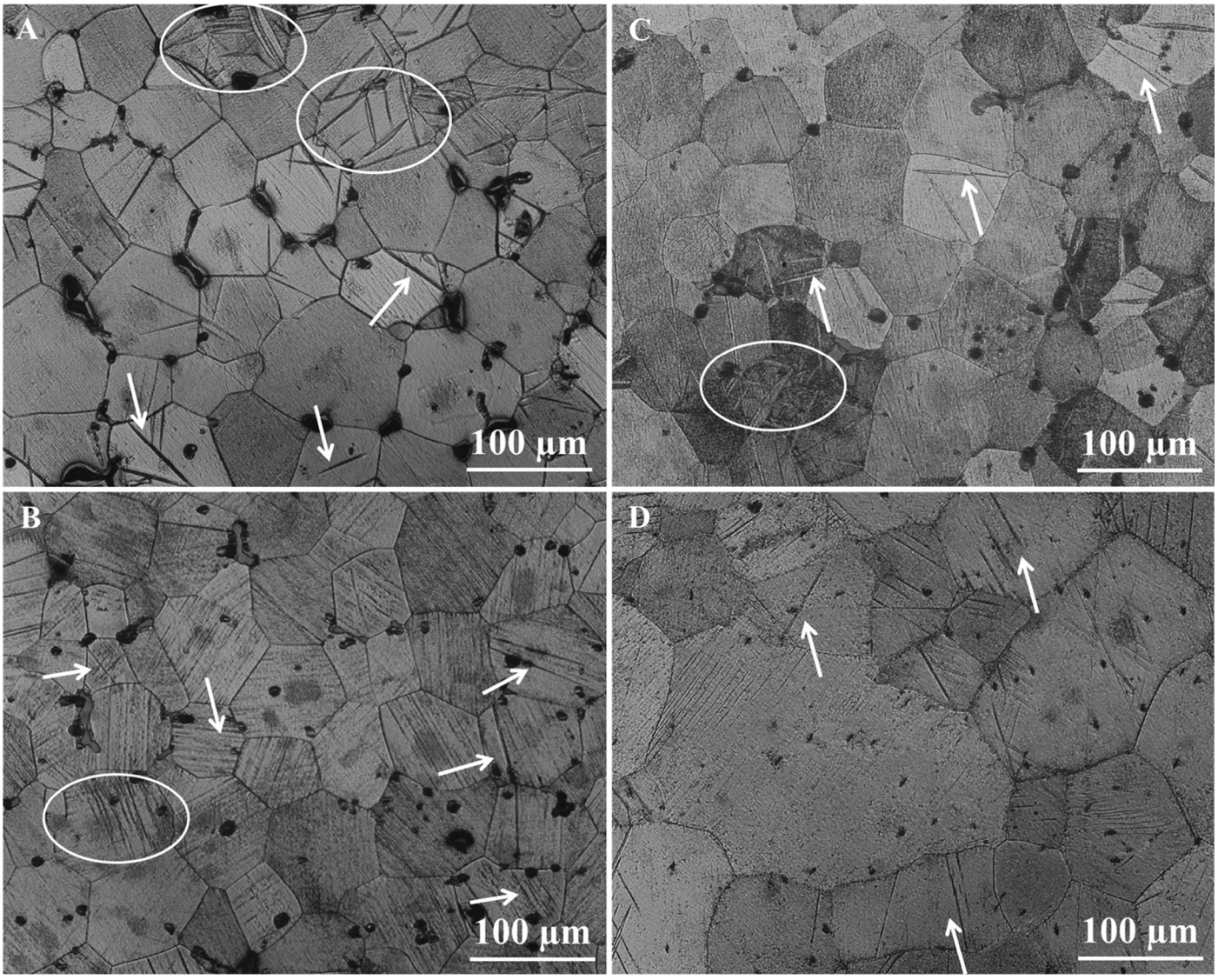

Fig. 5. Microstructures of QE22 alloy at different aging conditions: (A) solution treated (ST); (B) under aged (UA); (C) peak aged (PA); (D) over aged (OA); (twins are indicated with arrow heads and circle).

resulted in formation of deformation or mechanical twins in ST material. Mechanical twins are often observed in magnesium alloys because of HCP crystal structure due to non-availability of sufficient independent slip systems in order to satisfy the Von-Mises criterion [7]. However, mechanical twins are not thermally stable [14] and hence the levels of twins have reduced with respect to different aging conditions (UA, PA and OA).

To know the precipitate evolution during aging, TEM analysis was carried out on UA, PA and OA samples and shown in Fig. 6. TEM analysis of UA sample reveals the presence of fine spherical nano precipitates uniformly distributed inside and along the grains with an average size of 5 nm. These nano precipitates are most likely Guinier–Preston (GP) zones [12]. The TEM observation of PA sample shows the presence of uniformly distributed fine hexagonal/spherical precipitates with size ranging from 20 to 40 nm and few elongated precipitates. The hexagonal/spherical and elongated particles are β′ phase and λ phase precipitates respectively [8,9]. In case of OA sample, coarse particles are observed in TEM micrograph with dimensions in the range of 30–100 nm. These coarse particles are stable β phase precipitates which are having high thermal stability. Based on TEM analysis and existing literature [2–9,11], the precipitation evolution sequence in ST, UA, PA and OA samples can be concluded as follows:

$$\mathrm{SSSS\,(ST)} \rightarrow \mathrm{GP\ zone\ (UA)} \rightarrow \beta' + \lambda\,\mathrm{(PA)} \rightarrow \beta\,\mathrm{(OA)}$$

In summary, the solutes are dissolved in solid solution and retained as super saturated solid solution during ST. In UA state, evolution of GP zone occurs. At PA state these GP zones dissolve and evolution of a bimodal precipitation state consisting of β′ and λ phases occurs. On further aging up to OA condition, the λ phase precipitates dissolve completely and β′ phase precipitates transform to stable β precipitates.

The increasing trend of age hardening curve (64–87 Hv) up to 12 hours is due to the presence of coherent GP zones and

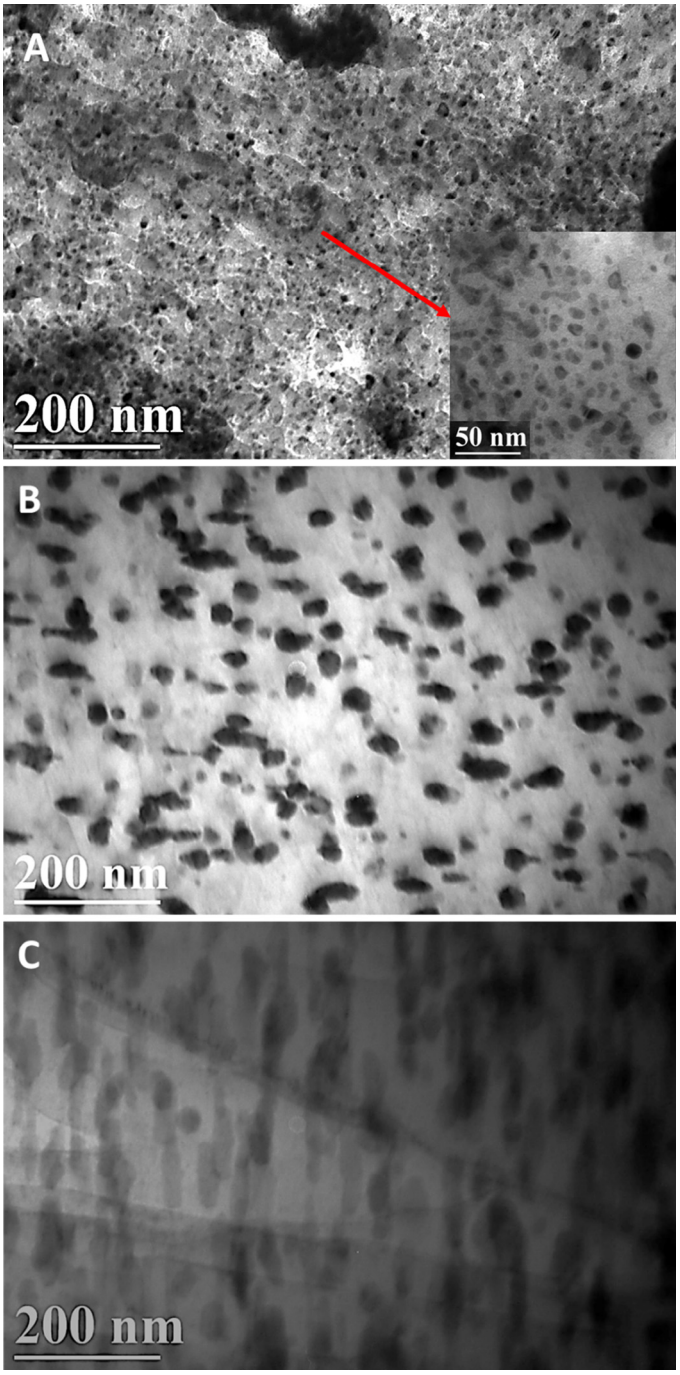

Fig. 6. Transmission electron microscopy of the QE22 at different aging conditions: (A) under aged (UA); (B) peak aged (PA); (C) over aged (OA).

transformation of GP zones to semi coherent β′ and coherent λ phase precipitates. After reaching peak aging condition, the hardness decreases from 87 Hv to 80 Hv at 50 hours and then almost saturates until 200 hours. The decrease in hardness at OA state is due to over aging effect because of the presence of incoherent stable β phase precipitates.

3.3. Tensile properties

The tensile properties (ultimate tensile strength (UTS), yield strength (YS) and elongation (ε)) of QE22 alloy in ST, UA, PA and OA conditions are presented in Fig. 7 and Table 3.

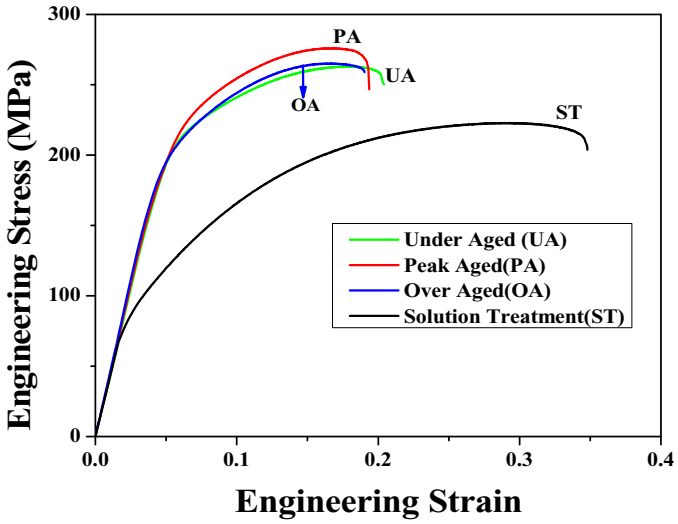

Fig. 7. Tensile properties (engineering stress vs. engineering strain) of QE22 alloy at different aging conditions.

Three important observations can be seen from Fig. 7 and Table 3 with respect to the strength and hardness properties in all the four thermal treated samples. First, the order of strength (both YS and UTS) improvement is PA > OA>UA > ST. The yield strength (YS), ultimate tensile strength (UTS) of the solution treated and peak aged QE22 alloy at room temperature are 80 MPa, 222 MPa and 199 MPa, 274 MPa respectively. The significant improvement of YS and UTS of PA sample as compared to ST sample is due to the presence of semi-coherent/coherent β′ and λ precipitate. The mechanical properties of UA, PA and OA samples are also observed as almost similar. The range of average YS, UTS and elongation (%) of UA, PA and OA is 195 ± 5 MPa, 263 ± 10 MPa and 13 ± 1% respectively.

The fractography analysis was carried on tensile fractured cross sections of ST, UA, PA and OA samples using scanning electron microscopy (SEM) and optical microscopy (OM) to study the failure analysis. Fig. 8 shows the optical microstructures of a tensile fractured surface of solution treated and thermal treated samples. In all the thermal treated samples except PA and OA conditions, the mode of failure was observed as transgranular (Fig. 8A and B). However, in the case of PA and OA treated samples, mixed mode of failure (transgranular and intergranular) was observed (Fig. 8C and D). This is due to the decorative action of eutectics and precipitates along the grain boundary.

The secondary electron (SE) micrographs of the fracture surfaces of the tensile specimens of QE22 alloy under various

Table 3
Hardness and tensile properties of QE22 alloy.

Sample condition	Hardness (Hv)	UTS (MPa)	YS (MPa)	ε (%)
Solution treated	64	222	80	30
Under aging	80	264	195	14
Peak aging	87	274	199	13
Over aging	73	266	197	12

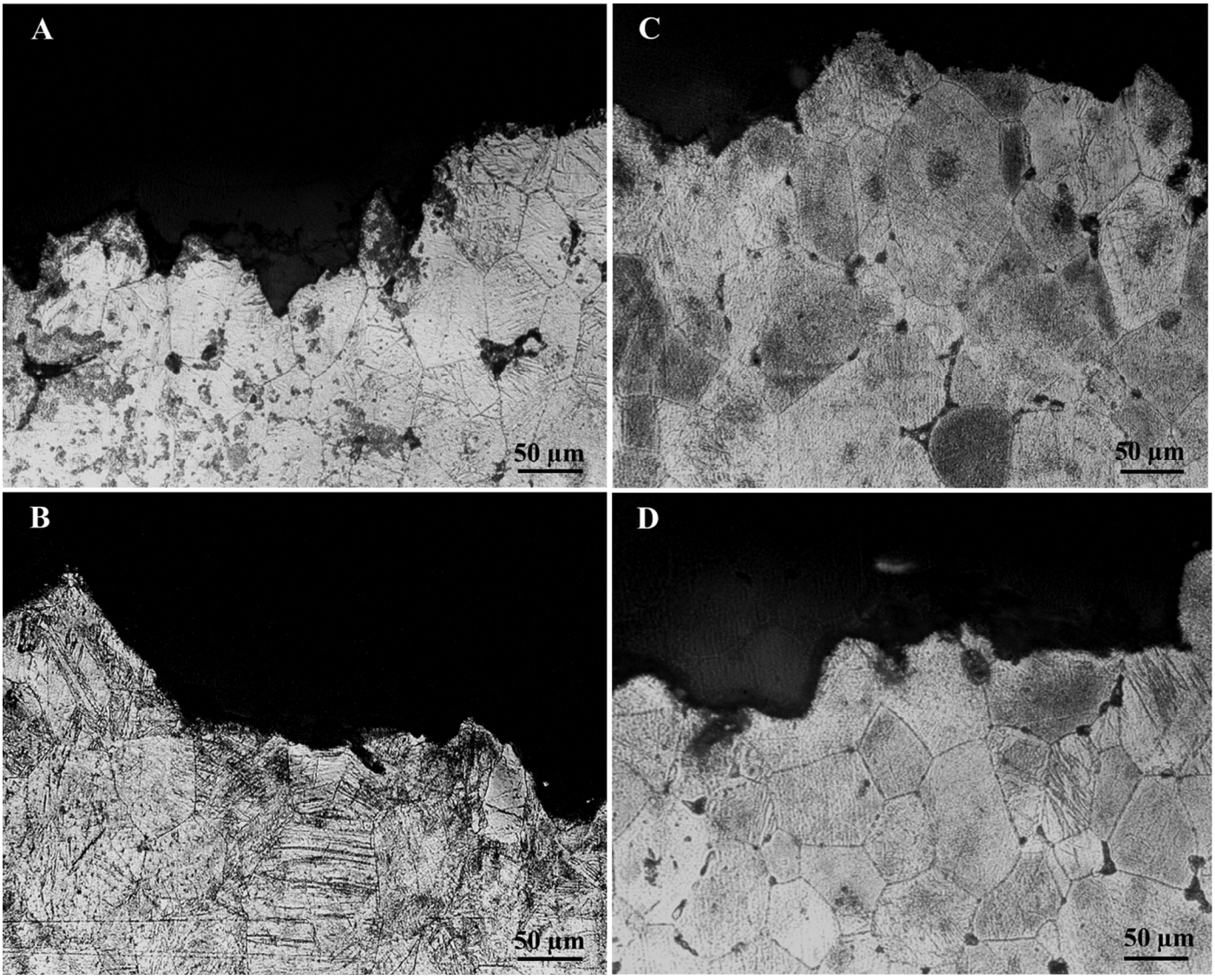

Fig. 8. Optical micrographs on tensile fracture surfaces of QE22 alloy at different aging conditions: (A) solution treated (ST); (B) under aged (UA); (C) peak aged (PA); (D) over aged (OA).

conditions are shown in Fig. 9. Twin boundary fracture is observed in all the processed (ST, UA, PA and OA) samples. Twinning is an important deformation mode in most of the HCP materials [3]. In solution treated sample, the fracture surfaces are mainly composed of ductile transgranular cleavage planes and tear ridges (Fig. 9A).The microstructure of the ST sample (Fig. 1) shows the presence of round shaped $Mg_{12}Nd$ eutectics along the grain boundaries and grain interiors. The XRD result shows the absence of ternary $Mg_{12}Nd_2Ag$ precipitates. Therefore, only $Mg_{12}Nd$ hard eutectic particles might have acted as crack nucleation points during tensile testing. Since the $Mg_{12}Nd$ eutectic particles are distributed at the grain interior and grain boundaries, the cracks might have initiated both at grain interiors and grain boundaries and propagated/traveled mainly transgranularly. Therefore, lots of cleavage planes are left on the fracture surface of ST samples which resulted high ductility (elongation: 30%). The nature of fracture mode of all the three age hardened samples (UA, PA and OA) is different than that of ST sample. The ductility of all the three aged samples is also lower than that of ST sample. In UA sample, the fracture surface is characterized mainly by cleavage planes and twin boundary fracture, as shown in Fig. 9B. A mixed pattern of transgranular, intergranular, cleavage planes and twin boundary fracture is observed in both PA and OA samples.

The precipitation sequence in the present QE22 alloy during aging is observed as SS α-Mg $\rightarrow$ *GP zones* $\rightarrow \beta' + \lambda \rightarrow \beta$ [2,9]. When the ST samples are subjected to precipitation hardening treatment, the intermediate precipitates are formed along the grain boundaries and grain interiors. As the age hardening time increases, the grain boundary precipitates become coarse and denser which has a tendency to reduce cohesive strength of the grain boundaries. This may result in favorable path for crack propagation. The UA sample has GP zones with 5 nm size which is uniformly distributed along the grains and grain

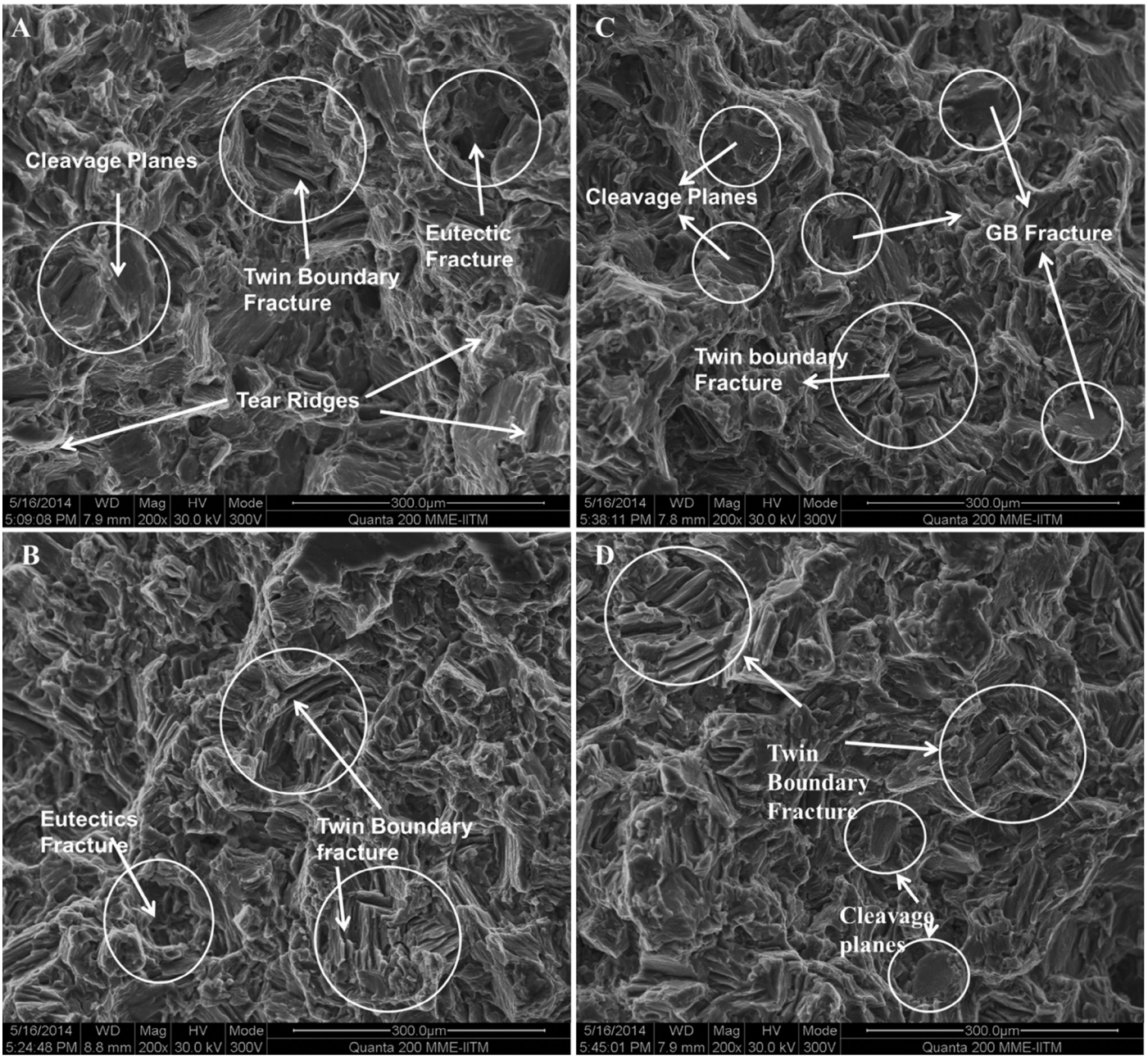

Fig. 9. Scanning electron microscopy of fracture surfaces after tensile testing of QE22 alloy at different aging conditions: (A) solution treated (ST); (B) under aged (UA); (C) peak aged (PA); (D) over aged (OA).

interiors (Fig. 6A). The strength of these tiny particles is not enough to reduce the cohesive strength of grain boundaries and resulted in cleavage transgranular fracture in UA sample. As the aging time increases to obtain PA treatment, the GP zones are transformed to semi coherent β′ and coherent λ phase precipitates and distributed along grain boundaries and grain interiors [4–6]. The density and shape of both types of precipitates along grain boundaries may be probably sufficient to reduce the grain boundary cohesive strength which resulted in intergranular fracture. The presence of precipitates at grain interiors and twins are responsible for transgranular failure. The grain boundary eutectic particles will be further responsible for both transgranular and intergranular failure. Therefore a mixed mode of transgranular and intergranular failure is observed in PA sample. Similar observation of failure mode as like PA sample is also observed in OA sample. A schematic diagram is shown in Fig. 10 which illustrates the failure mechanism of ST, UA, PA and OA samples.

A significant growth of grain size (GS of ST, UA and PA samples 50 ± 3 μm; GS of OA sample – 74 μm) and coarsening of precipitates (30–100 nm) are observed in OA sample (Fig. 6C). In spite of higher grain size and coarse precipitate, the ductility of OA sample is low. The possible reason is due to the presence of stable β phase particles with high density [4–6].

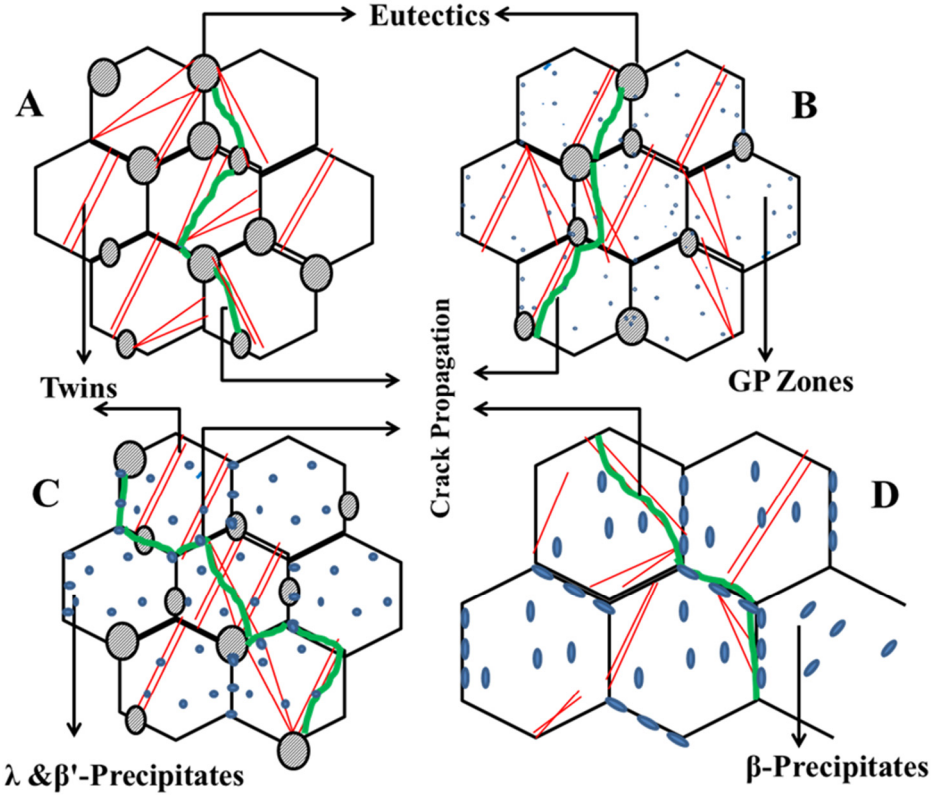

Fig. 10. Schematic diagrams showing the location of crack nucleation and propagation of QE22 alloy in different aging condition: (A) solution treated (ST); (B) under aged (UA); (C) peak aged (PA); (D) over aged (OA).

4. Conclusions

The microstructure, mechanical properties and fracture behavior of as-receivedMg-Ag-RE alloy (QE22) in different thermal conditions are analyzed and the following conclusions are made.

(1) The solution treated (ST), under aged (UA) and peak aged (PA) samples show high thermal stability with stable grain size in the range of 50 ± 3 μm. The possible cause for high thermal stability is due to the presence of $Mg_{12}Nd$ eutectics along the grain boundaries. Significant grain growth is observed in over aged (OA) samples (74 μm). During over aging, the eutectics as decorated along the grain boundary have been dissolved in the matrix which leads to grain growth.

(2) As compared to ST sample, the PA sample shows significant improvement of yield strength (YS) from 80 MPa to 222 MPa and ultimate tensile strength (UTS) from 199 MPa to 274 MPa. These improved mechanical properties are mainly associated with the metastable λ and β′ precipitates of $Mg_{12}Nd_2Ag$ phase.

(3) A significant reduction in ductility is observed in aged samples (UA: 14%, PA: 13% and OA: 12%) as compared to ST samples (30%). The reduction in ductility is due to the appearance of coherent precipitates of GP zones in UA sample, mixture of semi-coherent/coherent β′ and λ precipitates in PA sample and incoherent stable *β* precipitates in OA samples.

(4) The mode of failure of ST and UA samples was observed as transgranular. However, in the case of PA and OA samples, a mixed mode of failure (transgranular and intergranular) was observed. This is due to the presence of $Mg_{12}Nd$ eutectics along the grain boundaries and incoherent $Mg_{12}Nd_2Ag$ precipitates at grain interior and the grain boundaries.

References

[1] J. Kiehn, B. Smola, P. Vostry, I. Stulikova, K.U. Kainer, Phys. Stat. Sol. (A) 164 (1997) 709–723.
[2] J.F. Nie, Metallurg. Mater. Trans. A 43 (11) (2012) 3891–3939.
[3] S.K. Panigrahi, W. Yuan, R.S. Mishra, R. DeLorme, B. Davis, K. Cho, Mater. Sci. Eng. A 530 (2011) 28–35.
[4] L. Gao, R. Chen, E. Han, Trans. Nonfer. Met. Soc. China 20 (7) (2010) 1217–1221.
[5] F. Penghuai, P. Liming, J. Haiyan, Z. Zhenyan, Z. Chunquan, Mater. Sci. Eng. A 486 (1–2) (2008) 572–579.
[6] Q. Peng, H. Dong, Y. Wu, L. Wang, J. Alloys Comp. 456 (2008) 395–399.
[7] S.K. Panigrahi, K. Kumar, N. Kumar, W. Yuan, R.S. Mishra, R. DeLorme, et al., Mater. Sci. Eng. A 549 (2012) 123–127.
[8] G. Barucca, R. Ferragut, D. Lussana, P. Mengucci, F. Moia, G. Riontino, Acta Mater. 57 (15) (2009) 4416–4425.
[9] B.L. Mordike, Mater. Sci. Eng. A 324 (2002) 103–112.
[10] A. Kiełbus, J. Achievem. Mater. Manufact. Eng. 18 (1) (2006) 131–134.
[11] R. Ciach, A. Rakowska, M. Socjusz-podosek, L. Lityn, Mikrochim. Acta 149 (2002) 145–149.
[12] O.A. Lambri, W. Riehemann, Script. Mater. 52 (2) (2005) 93–97.
[13] I.J. Polmear, Mater. Trans. 37 (1) (1996) 12–31.
[14] H. Carpenter, S. Tamara, Proc. R. Soc. Lond. A Math. Phys. Sci. 113 (1926) 161.